Article:
Hardy, CM orcid.org/0000-0002-4550-4822, Livermore, PW orcid.org/0000-0001-7591-6716 and Niesen, J orcid.org/0000-0002-6693-3810 (2020) Enhanced magnetic fields within a stratified layer. Geophysical Journal International, 222 (3). pp. 1686-1703. ISSN 0956-540X

https://doi.org/10.1093/gji/ggaa260

Geophysical Journal International

Geophys. J. Int. (2020) **222,** 1686–1703
Advance Access publication 2020 May 28
GJI Geomagnetism, Rock Magnetism and Palaeomagnetism

doi: 10.1093/gji/ggaa260

Enhanced magnetic fields within a stratified layer

Colin M. Hardy [1], Philip W. Livermore [2] and Jitse Niesen [3]

[1] *EPSRC Centre for Doctoral Training in Fluid Dynamics, University of Leeds, Leeds, LS29JT, UK. E-mail: sccmh@leeds.ac.uk*
[2] *School of Earth and Environment, University of Leeds, Leeds LS29JT, UK*
[3] *School of Mathematics, University of Leeds, Leeds LS29JT, UK*

Accepted 2020 May 22. Received 2020 May 22; in original form 2020 January 3

SUMMARY

Mounting evidence from both seismology and numerical experiments on core composition suggests the existence of a layer of stably stratified fluid at the top of Earth's outer core. In such a layer, a magnetostrophic force balance and suppressed radial motion lead to stringent constraints on the magnetic field, named *Malkus constraints*, which are a much more restrictive extension of the well known Taylor constraints. Here, we explore the consequences of such constraints for the structure of the core's internal magnetic field. We provide a new simple derivation of these Malkus constraints, and show solutions exist which can be matched to any external potential field with arbitrary depth of stratified layer. From considerations of these magnetostatic Malkus constraints alone, it is therefore not possible to uniquely infer the depth of the stratified layer from external geomagnetic observations. We examine two models of the geomagnetic field defined within a spherical core, which obey the Taylor constraints in an inner convective region and the Malkus constraints in an outer stratified layer. When matched to a single-epoch geomagnetic potential field model, both models show that the toroidal magnetic field within the outer layer is about 100 times stronger compared to that in the inner region, taking a maximum value of 8 mT at a depth of 70 km. The dynamic regime of such a layer, modulated by suppressed radial motion but also a locally enhanced magnetic field, may therefore be quite distinct from that of any interior dynamo.

Key words: Composition and structure of the core; Core; Dynamo: theories and simulations.

1 INTRODUCTION

1.1 Stratification of Earth's core

The question of whether or not Earth's liquid outer core contains a stratified layer just below its outer boundary has long been debated (Braginsky 1967, 1987; Whaler 1980; Gubbins 2007; Hardy & Wong 2019). A stratified layer may result from the pooling of buoyant elements released from the freezing of the solid inner core (Braginsky 2006; Bouffard *et al.* 2019), diffusion from the mantle above (Jeanloz 1990; Buffett & Seagle 2010) or subadiabatic thermal effects (Pozzo *et al.* 2012). Within a strongly stratified layer, the dynamics would be very different to the remainder of the convecting core because spherical radial motion would be suppressed (Braginsky 1999; Davies *et al.* 2015; Cox *et al.* 2019). In terms of using observations of the changing internal geomagnetic field as a window on the dynamics within the core, the existence of a stratified layer is crucial because motion confined to the stratified layer such as waves may have a pronounced geomagnetic signature, which may be falsely interpreted as emanating from the large-scale dynamo process ongoing beneath.

Observational constraints on the stratified layer are largely from seismology, where analysis of a specific 'SmKS' class of waves has revealed a localized decrease in wave velocities in the outermost 100−300 km of the core (Lay & Young 1990; Helffrich & Kaneshima 2010, 2013), suggesting that the outermost part of the core has a different density and/or elasticity than the rest of the core. However, this evidence is far from conclusive because not all studies agree that a stratified layer is necessary to explain seismic measurements (Irving *et al.* 2018), and there are inherent uncertainties due to the remoteness of the core (Alexandrakis & Eaton 2010). So far, observational geomagnetism has offered equivocal evidence for stratified layers. Time dependent observational models can be explained by simple core flow structures on the core–mantle boundary (CMB) which have either no layer (Amit 2014; Holme 2015, upwelling at the CMB is permitted), or a strongly stratified layer (in which all radial motion is suppressed, Lesur *et al.* 2015).

A complementary approach to understanding the observational signature of a stratified layer is by numerical simulation of a stratified geodynamo model (Nakagawa 2011). Models of outer core dynamics have demonstrated that dynamo action can be sensitive to variations

in the assumed background state of a fully convective outer core, and that the presence of stably stratified layers can significantly alter the dynamics and morphology of the resultant magnetic field (Christensen 2018; Glane & Buffett 2018; Olson *et al.* 2018). Hence comparisons between the magnetic fields from stratified models with the geomagnetic field can be used to infer compatibility with the presence of a stratified layer. This has been used to constrain the possible thickness of a stratified layer such that it is consistent with geomagnetic observations. Yan & Stanley (2018) find that unstratified dynamo simulations significantly underpredict the octupolar component of the geomagnetic field. Their model endorses the presence of a thin stably stratified layer, as the resultant magnetic field can be rendered Earth-like by the inclusion of 60–130 km layer. However, the results are rather sensitive to both the strength of stratification and layer depth, with a thicker layer of 350 km resulting in an incompatible octupole field. Similarly Olson *et al.* (2017) find that stratified model results compare favourably with the time-averaged geomagnetic field for partial stratification in a thin layer of less than 400 km, but unfavourably for stratification in a thick 1000 km layer beneath the CMB. Additionally, in terms of dynamics, Braginsky (1993) and Buffett (2014) show that MAC [Magnetic, buoyancy (Archimedean) and Coriolis forces] waves in the *hidden ocean* at the top of the core provide a mechanism for the 60-yr-period oscillations detected in the geomagnetic field (Roberts *et al.* 2007). The model of Buffett *et al.* (2016) suggests that MAC waves underneath the CMB are also able to account for a significant part of the fluctuations in length of day (LOD, Gross 2001; Holme & De Viron 2005) through explaining the dipole variation, but are contingent on the existence of a stratified layer at the top of the core with a thickness of at least 100 km. However, not all stratified dynamo model results champion this scenario for the Earth. It has been found that the inclusion of a thin stable layer in numerical models can act to destabilize the dynamo, through generating a thermal wind which creates a different differential rotation pattern in the core (Stanley & Mohammadi 2008). Additionally many distinctive features of the geomagnetic field are not reproduced, as strong stratification leads to the disappearance of reverse flux patches and suppression of all non-axisymmetric magnetic field components (Christensen & Wicht 2008; Mound *et al.* 2019).

1.2 The Earth-like magnetostrophic force balance

One reason why there is no clear message from existing geodynamo models is perhaps that they all have been run in parameter regimes very far from Earth's core (Roberts & Aurnou 2011). Two important parameters, the Ekman and Rossby numbers, quantify the ratio of rotational to viscous forces $E \sim 10^{-15}$ and the ratio of inertial to viscous forces $R_o \sim 10^{-7}$, respectively (Christensen & Wicht 2015). These parameters being so small causes difficulties when attempting to numerically simulate the geodynamo because they lead to small spatial and temporal scales that need to be resolved in any direct numerical simulation, but are extremely computationally expensive to do so. Despite this challenge, numerical models have been used with great success to simulate aspects of the geodynamo, reproducing features such as torsional oscillations (Wicht & Christensen 2010) that are consistent with observational models (Gillet *et al.* 2010), geomagnetic jerks (Aubert & Finlay 2019) and allowing predictions of the Earth's magnetic field strength (Christensen *et al.* 2009). Recent simulations have been able to probe more Earth-like parameter regimes than previously possible, achieving very low Ekman numbers of $E = 10^{-7}-10^{-8}$ (Schaeffer *et al.* 2017; Aubert 2019). However despite this progress, these simulations remain in parameter regimes vastly different to that of the Earth (Christensen & Wicht 2015), posing the inescapable question of how representative of the Earth they really are, as force balances can still vary significantly between the simulation regime and the correct regime of the Earth (Wicht & Sanchez 2019), with the ability to simultaneously reproduce Earth-like field morphology and reversal frequency still beyond current capabilities (Christensen *et al.* 2010). The assessments conducted by Sprain *et al.* (2019) highlight that present geodynamo models are unable to satisfactorily reproduce all aspects of Earth's long-term field behaviour.

Another approach to estimate the magnetic state within the core is by using data assimilation, through which the rapidly changing dynamics and surface field from geodynamo simulations and observational data, respectively, can be used to infer the interior core dynamics and magnetic field (e.g. Fournier *et al.* 2007). The principle is to seek the most likely core state that accounts for the observed magnetic field, while being statistically compliant with the output of a numerical model of the geodynamo. This has been implemented by, for example, Aubert & Fournier (2011) and Aubert (2012, 2014) for a fully convective core. However the existence of a stratified layer has obvious implications for the applicability to Earth, as this approach is founded on observations at the CMB matching those of of the modelled core's outer edge: any stratified layer would provide a disconnect between these two. Questions remain over how the force balance may differ within a stratified layer, and importantly whether any classes of externally observable magnetic field are incompatible with a stratified layer. We are able to address this through considering whether all structures of exterior potential fields are consistent with an assumed magnetostrophic balance and the presence of a strongly stratified layer.

In this paper, we adopt an approach of consider from a theoretical standpoint the structure of the geomagnetic field within any such strongly stratified layer. Our starting point is the model of Taylor (1963), based on the assumption that the inertia-free and viscosity-free asymptotic limit is more faithful to Earth's dynamo than adopting numerically expedient but nevertheless inflated parameter values. This amounts to setting the values of R_o and E to zero, which simplifies the governing equations significantly, enabling numerical solutions at less computational expense and importantly for us, analytic progress to be made. The resulting dimensionless magnetostrophic regime then involves an exact balance between the Coriolis force, pressure, buoyancy and the Lorentz force associated with the magnetic field **B** itself:

$$\hat{\boldsymbol{z}} \times \boldsymbol{u} = -\nabla p + F_B \hat{\boldsymbol{r}} + (\nabla \times \boldsymbol{B}) \times \boldsymbol{B}, \tag{1}$$

where F_B is a buoyancy term that acts in the unit radial direction $\hat{\boldsymbol{r}}$ (Fearn 1998). Throughout this paper we consider the magnetostrophic balance of eq. (1).

1.3 Constraints on the magnetic field

Taylor (1963) showed that, as a consequence of this magnetostrophic balance, the magnetic field must obey at all times t the well-known condition

$$T(s,t) \equiv \int_{C(s)} ((\nabla \times \mathbf{B}) \times \mathbf{B})_\phi \, s \mathrm{d}\phi \mathrm{d}z = 0, \tag{2}$$

for any geostrophic cylinder $C(s)$ of radius s, aligned with the rotation axis, where (s, ϕ, z) are cylindrical coordinates. This constraint applies in the general case for fluids independent of stratification. It was first shown by Malkus (1979) how (2) can be refined within a stratified layer of constant depth, which in the limit of zero radial flow leads to a more strict constraint. This constraint now applies on every axisymmetric ring coaxial with the rotation axis that lies within the layer and is known as the *Malkus constraint*

$$M(s,z,t) \equiv \int_0^{2\pi} ((\nabla \times \boldsymbol{B}) \times \boldsymbol{B})_\phi \, \mathrm{d}\phi = 0,$$

for any s and z within the layer; thus for the stratified case a single Taylor constraint on a cylinder transforms into an infinite number of Malkus constraints. Magnetic fields that satisfy the Taylor or Malkus constraints respectively are termed Taylor or Malkus states.

The associated timescale over which the dominant force balance described by the magnetostrophic equations evolves is $\sim 10^4$ yr. However observations show changes in the geomagnetic field on much shorter timescale of years to decades (Jackson & Finlay 2015). This vast discrepancy in timescales motivates distinguishing between the slowly evolving background state and perturbations from it and considering these two features separately. The theoretically predicted magnetostrophic timescale, represented by Taylor or Malkus states, describes the slow evolution of the magnetic field, and may explain dynamics such as geomagnetic reversals and also the longstanding dominance of the axially symmetric dipolar component of the field. Although rapid dynamics such as MHD waves occur on a much shorter timescale, they cannot be considered in isolation as their structure depends critically upon the background state that they perturb. Thus although insightful models of perturbations can be based upon simple states (e.g. Malkus 1967), ultimately a close fit to the observed geomagnetic field requires accurate knowledge of the background state. It is the search for such a state that is explored in this paper.

Dynamic models of a non-stratified background state, produced by evolving the magnetic field subject to Taylor's constraint, have appeared very recently (Wu & Roberts 2015; Li *et al.* 2018; Roberts & Wu 2018) and are currently restricted to axisymmetry, although the model of Li *et al.* (2018) can be simply extended to a three dimensional system. These models can additionally be used to probe the effect of incorporating inertia driven torsional waves within this framework (Roberts & Wu 2014).

In this paper, we explore the use of both the Taylor and Malkus constraints as a tool for probing instantaneous structures of the magnetic field throughout Earth's core. This method ignores any dynamics and asks simply whether we can find a set of magnetic fields which satisfy the necessary constraints. Our task is a challenging one: even finding magnetic fields that exactly satisfy the comparatively simple case of Taylor's constraint has proven to be difficult in the 55 yr since the seminal paper of Taylor (1963), although notable progress has been made in axisymmetry (Soward & Jones 1983; Hollerbach & Ierley 1991) and in 3-D (Jault & Cardin 1999) subject to imposing a specific symmetry. Recently, significant progress has been made in this regard by presenting a more general understanding of the mathematical structure of Taylor's constraint in three dimensions (Livermore *et al.* 2008). This method was implemented by Livermore *et al.* (2009) to construct simple, large scale magnetic fields compatible with geomagnetic observations. It is this which provides the foundation for the work presented here.

1.4 Objectives

While exploring the theoretical implications of the Malkus constraints, we will aim to address the following objectives which originally motivated this work:

(i)Do exact or approximate Malkus states exist? It is not *a priori* obvious whether or not there are enough degrees of freedom within any magnetic field to satisfy all required constraints.
(ii)Does any snapshot of the geomagnetic field convey information about whether there is a strongly stratified layer at the top of the core?
(iii)What might be the present-day internal structure of the geomagnetic field inside a stratified layer?

The remainder of this paper is structured as follows. In Section 2, we present a new, more general derivation of the condition required to be satisfied with a stratified layer of fluid, which under an idealized limit reduces to what is known as Malkus' constraint. In Sections 3–5, we summarize a method for constructing Malkus states, applying it to a snapshot of the present day field in Sections 6 and 7; we conclude in Section 8.

2 DERIVATION OF MALKUS' CONSTRAINT

Within stably stratified fluids radial flows are suppressed, hence in the limit of strong stratification radial fluid velocities are negligibly small (Braginsky 1999; Davies *et al.* 2015). We proceed within this idealistic limit and require that $u_r = 0$ within a region of stratified fluid that is a volume of revolution: we represent the proposed stratified layer within Earth's core as a spherically symmetric layer of constant depth. We assume further that the system is in magnetostrophic balance; that is, rapidly rotating with negligible inertia and viscosity. The resulting

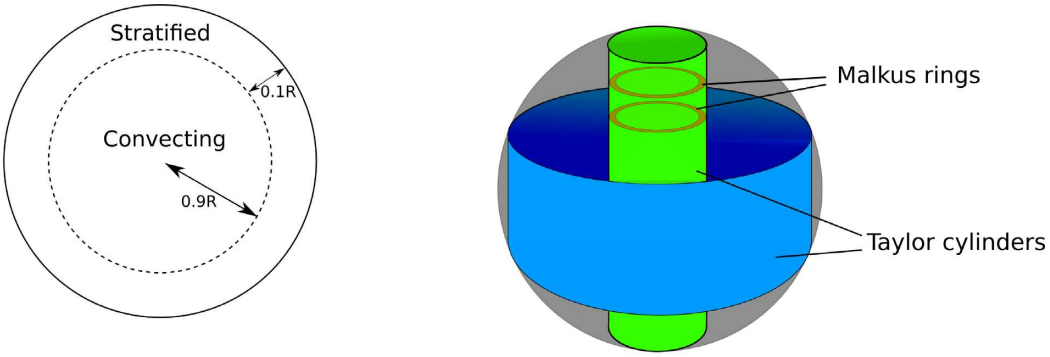

Figure 1. (a) Earth-like spherical shell with radius $r_{SL} = 0.9R$. A Malkus state defined in a stratified layer surrounds an interior Taylor state. (b) Geometry of constraint surfaces.

constraint was first derived by Malkus (1979), however, here we present an alternative and more straightforward derivation courtesy of Dominique Jault (personal communication).

We use the condition for incompressible flow that $\nabla \cdot \boldsymbol{u} = 0$ and the standard toroidal poloidal decomposition within spherical coordinates (r, θ, ϕ). From the condition that there is no spherically radial component of velocity then $\boldsymbol{u}$ must be purely toroidal and hence can be written as

$$\boldsymbol{u} = \nabla \times (\mathcal{T}(r, \theta, \phi)\hat{\boldsymbol{r}}) = \frac{1}{r \sin\theta} \frac{\partial \mathcal{T}}{\partial \phi} \hat{\boldsymbol{\theta}} - \frac{1}{r} \frac{\partial \mathcal{T}}{\partial \theta} \hat{\boldsymbol{\phi}}.$$

Therefore the cylindrically radial velocity, written in spherical coordinates, is

$$u_s = \sin\theta u_r + \cos\theta u_\theta = \frac{\cos\theta}{r \sin\theta} \frac{\partial \mathcal{T}}{\partial \phi}$$

and so

$$\int_0^{2\pi} u_s \, \mathrm{d}\phi = \frac{\cos\theta}{r \sin\theta} \int_0^{2\pi} \frac{\partial \mathcal{T}}{\partial \phi} \, \mathrm{d}\phi = 0.$$

Now, since $\hat{\boldsymbol{\phi}} \cdot (\hat{\mathbf{z}} \times \boldsymbol{u}) = u_s$ then, from the azimuthal component of the magnetostrophic eq. (1) we have

$$u_s = -\frac{\partial p}{\partial \phi} + ((\nabla \times \boldsymbol{B}) \times \boldsymbol{B})_\phi.$$

Integrating in ϕ around any circle of constant (s, z) , as illustrated by the red rings in Fig. 1, and using the single-valued nature of pressure, gives Malkus' constraint,

$$\underbrace{\int_0^{2\pi} u_s \, \mathrm{d}\phi}_{=0} = -\underbrace{\int_0^{2\pi} \frac{\partial p}{\partial \phi} \, \mathrm{d}\phi}_{=0} + \int_0^{2\pi} ((\nabla \times \boldsymbol{B}) \times \boldsymbol{B})_\phi \, \mathrm{d}\phi = 0,$$

or equivalently requiring that the Malkus integral M is zero:

$$M(s, z, t) \equiv \int_0^{2\pi} ((\nabla \times \boldsymbol{B}) \times \boldsymbol{B})_\phi \, \mathrm{d}\phi = 0. \tag{3}$$

We are also able to generalize this constraint from considering the idealistic limit of requiring $u_r = 0$ within the stratified fluid to the more general situation of permitting $u_r \neq 0$, where we express the Malkus integral in terms of the radial flow. Now, the flow **u** is no longer purely toroidal and hence

$$M(s, z, t) = \int_0^{2\pi} u_s \, \mathrm{d}\phi = \int_0^{2\pi} u_\theta \cos\theta \mathrm{d}\phi + \int_0^{2\pi} u_r \sin\theta \, \mathrm{d}\phi. \tag{4}$$

We now use the condition for incompressible flow that $\nabla \cdot \boldsymbol{u} = 0$,

$$0 = \nabla \cdot \mathbf{u} = \frac{1}{r^2} \frac{\partial (r^2 u_r)}{\partial r} + \frac{1}{r \sin\theta} \frac{\partial (u_\theta \sin\theta)}{\partial \theta} + \frac{1}{r \sin\theta} \frac{\partial u_\phi}{\partial \phi},$$

$$\Rightarrow \int_0^{2\pi} \left(\frac{\sin\theta}{r} \frac{\partial (r^2 u_r)}{\partial r} + \frac{\partial (u_\theta \sin\theta)}{\partial \theta} \right) \mathrm{d}\phi = -\int_0^{2\pi} \frac{\partial u_\phi}{\partial \phi} \mathrm{d}\phi = 0.$$

Now integrating over $[0, \theta]$ we find

$$\int_0^{2\pi} u_\theta \mathrm{d}\phi = \frac{1}{\sin\theta} \int_0^\theta \frac{\sin\theta'}{r} \int_0^{2\pi} \frac{\partial (r^2 u_r)}{\partial r} \mathrm{d}\phi \mathrm{d}\theta' = -\frac{1}{r \sin\theta} \int_0^\theta \sin\theta' \frac{\partial}{\partial r} \left(r^2 \int_0^{2\pi} u_r \mathrm{d}\phi \right) \mathrm{d}\theta'$$

$$\Rightarrow M = -\frac{1}{r\tan\theta}\int_0^{\theta}\frac{\partial}{\partial r}\left(r^2\int_0^{2\pi}u_r\sin\theta'\,\mathrm{d}\phi\right)\mathrm{d}\theta' + \int_0^{2\pi}u_r\sin\theta\,\mathrm{d}\phi.$$

In the above derivation, no assumption has been made about stratification and this equation holds as an identity in the magnetostrophic regime independent of stratification. In the case considered by Malkus, $M = 0$ is recovered in the limit of $u_r \to 0$.

It is clear that Malkus' constraint is similar to Taylor's constraint except now not only does the azimuthal component of the Lorentz force need to have zero average over fluid cylinders, it needs to be zero for the infinite set of constant-z slices of these cylinders (here termed *Malkus rings*, see Fig. 1) that lie within the stratified region. In terms of the flow, the increased restriction of the Malkus constraint arises because it requires zero azimuthally averaged u_s at any given value of z, whereas Taylor's constraint requires only that the cylindrically averaged u_s vanishes and allows outward flow at a given height to be compensated by inward flow at another. We note that all Malkus states are Taylor states, but the converse is not true.

3 GEOMETRY AND REPRESENTATION OF A STRATIFIED MAGNETOSTROPHIC MODEL

The physical motivation for applying Malkus' constraint arises from seeking to find a realistic model for the magnetic field in the proposed stratified layer within Earth's outer core. Hence we compute solutions for the magnetic field in the Earth-like configuration illustrated in Fig. 1(a), consisting of a spherical region in which Taylor's constraint applies, representing the inner convective region of Earth's core, surrounded by a spherical shell in which Malkus' constraint applies, representing the stratified layer immediately beneath the CMB. Our method allows a free choice of inner radius $r_{\rm SL}$; in order to agree with the bulk of seismic evidence (Lay & Young 1990; Helffrich & Kaneshima 2010, 2013), the value $r_{\rm SL} = 0.9R$ is chosen for the majority of our solutions, where R is the full radius of the core (3845 km). However due to the uncertainty which exists for the thickness of Earth's stratified layer (Kaneshima 2017), we also probe how sensitive our results are to layer thickness, considering $r_{\rm SL} = 0.5R,\ 0.85R,\ 0.95R,\ 0.99R$ and $0.999R$ as well. The Earth's inner core is neglected throughout, since incorporating it would lead to additional intricacies due to the cylindrical nature of Taylor's constraint which leads to a distinction between regions inside and outside the tangent cylinder (Livermore & Hollerbach 2012; Livermore *et al.* 2008; Roberts & Wu 2020). Since the focus here is on the outermost reaches of the core, we avoid such complications.

The method used to construct the total solution for the magnetic field throughout Earth's core that is consistent with the Taylor and Malkus constraints is sequential. Firstly, we use a regular representation of the form shown in eq. (7) to construct a Malkus state in the stratified layer. Secondly, we construct a Taylor state which matches to the Malkus state at $r = r_{\rm SL}$; overall the magnetic field is continuous but may have discontinuous derivatives on $r = r_{\rm SL}$. We note that any flow driven by this magnetic field through the magnetostrophic balance may also be discontinuous at $r = r_{\rm SL}$ because in general $u_r \neq 0$ in the inner region but $u_r = 0$ is assumed in the stratified region. Considerations of such dynamics lie outside the scope of the present study focused only on the magnetic constraints, but imposing continuity of u_r for example would clearly require additional constraints.

As a pedagogical exercise we also construct some Malkus states within a fully stratified sphere ($r_{\rm SL} = 0$), as detailed in Appendix A. Without the complications of matching to a Taylor state, the equations take a simpler form and we present some first examples in Appendix A2. Dynamically, sustenance of a magnetic field within a fully stratified sphere is of course ruled out by the theory of Busse (1975), which provides a strictly positive lower bound for the radial flow as a condition on the existence of a dynamo. Nonetheless it can be insightful to first consider the full sphere case, as it facilitates the consideration of fundamental principles of the magnetic field and Malkus constraint structure, and allows direct comparisons to be made with similar full sphere Taylor states.

In what follows we represent a magnetic field by a sum of toroidal and poloidal modes with specific coefficients

$$\boldsymbol{B} = \sum_{l=1}^{L_{max}}\sum_{m=-l}^{l}\sum_{n=1}^{N_{max}} a^m_{l,n}\boldsymbol{\mathcal{T}}^m_{l,n} + b^m_{l,n}\boldsymbol{\mathcal{S}}^m_{l,n}, \tag{5}$$

where $\boldsymbol{\mathcal{T}}^m_{l,n} = \boldsymbol{\nabla}\times(T_{l,n}(r)Y^m_l\hat{\mathbf{r}})$, $\boldsymbol{\mathcal{S}}^m_{l,n} = \boldsymbol{\nabla}\times\boldsymbol{\nabla}\times(S_{l,n}(r)Y^m_l\hat{\mathbf{r}})$, $N_{\rm max}$ is the radial truncation of the poloidal and toroidal field. In the above, Y^m_l is a spherical harmonic of degree l and order m, normalized to unity by its squared integral over solid angle. Positive or negative values of m indicate, respectively, a $\cos m\phi$ or $\sin m\phi$ dependence in azimuth. The scalar functions $T^m_{l,n}$ and $S^m_{l,n}$, $n \geq 1$, are respectively, chosen to be the functions $\chi_{l,n}$ and $\psi_{l,n}$ composed of Jacobi polynomials (Li *et al.* 2010, 2011). They are orthogonal, and obey regularity conditions at the origin and the electrically insulating boundary condition at $r = R$

$$\frac{\mathrm{d}\mathcal{S}^m_l}{\mathrm{d}r} + l\mathcal{S}^m_l/R = \mathcal{T}^m_l = 0. \tag{6}$$

We note that this description is convenient but incomplete when used within the spherical shell, for which the magnetic field does not need to obey regularity at the origin. For simplicity, we nevertheless use this representation in both layers, although restricting the domain of the radial representation to $[0, r_{\rm SL}]$ for the inner region.

4 DISCRETIZATION OF THE CONSTRAINTS

4.1 The Taylor constraints

Since the Malkus constraint forms a more restrictive constraint which encompasses the Taylor constraint it is useful for us to first summarize the structure of the Taylor constraint in a full sphere. The integral given in eq. (2), which Taylor's constraint requires to be zero, is known as the Taylor integral. Although applied on an infinite set of surfaces, Livermore *et al.* (2008) showed that Taylor's constraint reduces to a finite number of constraint equations for a suitably truncated magnetic field expansion

$$\mathcal{S}_l^m(r) = r^{l+1}\sum_{j=0}^{N_{max}} c_j r^{2j} \quad \text{and} \quad \mathcal{T}_l^m(r) = r^{l+1}\sum_{j=0}^{N_{max}} d_j r^{2j}, \tag{7}$$

which is an expanded version of (5) for some c_j and d_j. The Taylor integral itself then collapses to a polynomial of finite degree which depends upon s^2 (Lewis & Bellan 1990) and the coefficients $a_{l,n}^m$, $b_{l,n}^m$, and takes the form

$$T(s) = s^2\sqrt{R-s^2}\,Q_{D_T}(s^2) = 0, \tag{8}$$

for some polynomial Q_{D_T} of maximum degree D_T.

Taylor's constraint is now equivalent to enforcing that the coefficients of all powers of s in the polynomial Q_{D_T} equal zero, as this ensures $T(s)$ vanishes identically on every geostrophic contour. This translates into $C_T = L_{\max} + 2N_{\max} - 2$ conditions after the single degeneracy due to the electrically insulating boundary condition is removed (Livermore *et al.* 2008), transforming the infinite number of constraints to a finite number of simultaneous, coupled, quadratic, homogeneous equations. This reduction is vital as it gives a procedure for enforcing Taylor's constraint in general, and allows the implementation of a method to construct magnetic fields which exactly satisfy this constraint, known as Taylor states, as demonstrated by Livermore *et al.* (2009). In the next section we see how, with some relatively simple alterations this procedure can be extended to the construction of exact Malkus states.

4.2 The Malkus constraints

Along similar lines as we showed for Taylor's constraints, we now outline some general properties of the mathematical structure of Malkus' constraints. On adopting the representation (5) the Malkus integral reduces to a multinomial in s^2 and z (Lewis & Bellan 1990) and we require

$$M(s,z) = Q_{D_M}(s^2, z) = 0$$

for some finite degree multinomial Q_{D_M} in s and z. Note that the Taylor integral (8) is simply a z-integrated form of Q_{D_M}. Equating every multinomial term in $Q_{D_M}(s^2, z)$ to zero results in a finite set of constraints that are non-linear in the coefficients $a_{l,n}^m$ and $b_{l,n}^m$.

The number of constraints can be quantified for a given truncation following a similar approach as that used by Livermore *et al.* (2008) for Taylor's constraint, by tracking the greatest exponent of the dimension of length. This analysis is conducted in Appendix C and results in the number of Malkus constraints given by

$$C_M = {C_T}^2 + 3C_T + 2. \tag{9}$$

Therefore we find that as expected the Malkus' constraints are more numerous than Taylor's constraints. It is significant to notice that $C_M \gg C_T$ and in particular for high degree/resolution systems $C_M \approx {C_T}^2$.

In order to satisfy these constraints, the magnetic field has $2L_{\max}N_{\max}(L_{\max}+2)$ degrees of freedom (this being the number of unknown spectral coefficients within the truncation of $(L_{\max}, N_{\max})$. In axisymmetry the number of degrees of freedom reduces to $2N_{\max}L_{\max}$.

If we truncate the magnetic field quasi uniformly as $N = \mathcal{O}(L_{\max}) \approx \mathcal{O}(N_{\max})$, then we observe that at high N the number of constraints [$O(N^2)$ Malkus constraints; $O(N)$ Taylor constraints] is exceeded by the number of degrees of freedom of N^3. A simple argument based on linear algebra suggests that many solutions (for both Taylor and Malkus states) exist at high N, however this may be misleading because the constraints are non-linear and it is not obvious *a priori* whether any solutions exist, or if they do, how numerous they might be. We discuss this further in the next section.

Finally, we present a simple example in Appendix A1, which shows the structure of constraint equations that arise. The example highlights that many of the Malkus constraints are linearly dependent: the constraint degeneracy plays a far more significant role for the Malkus constraints compared with the Taylor constraints, which only have a single weak degeneracy due to the electrically insulating boundary condition (Livermore *et al.* 2008). While this degeneracy effectively lowers the number of constraints (making it easier to find a solution), due to the complex nature of the non-linear equations at present we have no predictive theory for the total number of independent constraints.

5 EXISTENCE OF MALKUS STATES

In this section, we directly address the first of our objectives: do Malkus states exist? We proceed in two parts. First, we give some analytic examples of non-geophysical but simple and exact Malkus states. Second, we show how a Malkus state can be constructed that matches any exterior potential field, thereby markedly extending the class of known Malkus states.

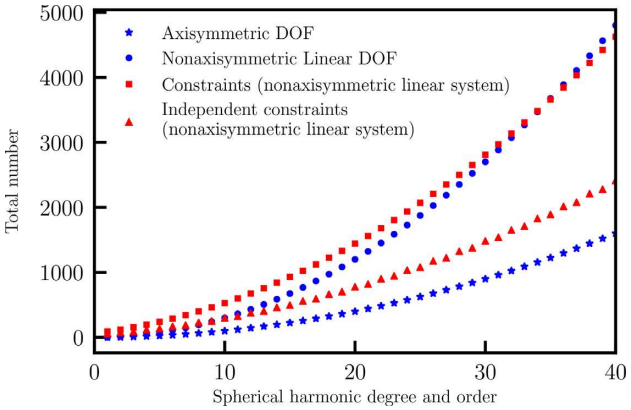

Figure 2. This graph compares the number of constraints to degrees of freedom (DOF) as a function of toroidal field spherical harmonic resolution with $L_{\max} = N_{\max}$, given a fixed poloidal field of $L_{\max} = 13$. This illustrates that for the non-axisymmetric linear system we construct then the number of degrees of freedom (red) exceeds the number of independent constraints (red triangles) for a toroidal field of resolution $L_{\max} = N_{\max} \geq 10$.

5.1 Simple analytic states

Simple Malkus states may be constructed by exploiting the analytic form of the integrand defining the Malkus constraint (see Appendix B) and the symmetries inherent in the spherical harmonics that define our basis representation for the magnetic field. In order of simplicity, we present a list of some simple Malkus states:

(1)Any magnetic field based on a single spherical harmonic because of symmetry in the azimuthal integration.
(2)Any axisymmetric purely toroidal or poloidal field since the integrand itself $((\nabla \times \mathbf{B}) \times \mathbf{B})_\phi$ is zero.
(3)Equatorially symmetric purely toroidal or poloidal field comprising either only cosine or only sine dependence in azimuth, as the resultant integrand is antisymmetric with respect to a rotation of π radians in azimuth and hence vanishes under azimuthal integration over $[0, 2\pi]$.

The last example plays an important role in the more general discussion of Malkus states (and see Appendix B).

5.2 General Malkus states

We now investigate whether it is possible to find much more general Malkus states; specifically we address whether we can find a Malkus state that matches at the edge of the core any given exterior potential magnetic field

$$\mathbf{B}_{ext} = -\nabla V; \qquad V = R \sum_{l=1}^{L_{max}} \sum_{m=0}^{l} \left(\frac{R}{r}\right)^{l+1} (g_l^m \cos(m\phi) + h_l^m \sin(m\phi)) P_l^m(\cos\theta), \tag{10}$$

where P_l^m is an associated Legendre polynomial and g_l^m and h_l^m are the Gauss coefficients.

In the following, we set out one procedure for finding such a Malkus state. Following the method of Livermore *et al.* (2009) which describes how to find analogous Taylor states, we completely specify the poloidal field within the core, downwards continuing the exterior potential field inside the core $r \leq R$ by assuming a profile for each poloidal harmonic of degree l that minimizes the Ohmic dissipation within the modelled core, compatible both with an electrically insulating outer boundary and regularity at the origin (Backus *et al.* 1996):

$$(2l+3)r^{l+1} - (2l+1)r^{l+3}. \tag{11}$$

Because the core's toroidal field is hidden from external view, we are now free to choose it without affecting the matching to $\mathbf{B}_{\text{ext}}$. The question is two fold: whether there are sufficient degrees of freedom in the toroidal field to exceed the number of independent nonlinear constraints, and whether a solution can be found. These issues are addressed in Appendix B, where it is shown that it is indeed possible to find such a toroidal field that renders any given poloidal field a Malkus state, by identifying a judicious choice of toroidal modes which result in a linear (rather than a non-linear) system whose solution is then straightforward.

Fig. 2 shows the existence of such solutions through providing a specific example of the number of constraints given $\mathbf{B}_{\text{ext}}$ of degree 13. It demonstrates three important things. Firstly, that due to degeneracy the independent linear constraints (red triangles) are much fewer than the full set of linear constraints (red squares). Secondly, that the number of degrees of freedom exceed the number of independent constraints at $L_{\max} = N_{\max} \geq 10$ if we consider our preferred non-axisymmetric toroidal basis (of Appendix B, blue circles); in particular if we adopt a toroidal field of the same degree as the poloidal field $L_{\max} = N_{\max} = 13$ then we find an infinite set of Malkus states. Thirdly, a laterally complex toroidal field is required to find a Malkus state. Here this is demonstrated by the fact that any attempt to find a Malkus state by adding to the poloidal field an axisymmetric toroidal field will fail, because the number of degrees of freedom (blue stars) is always exceeded by the number of independent constraints .

Having found a Malkus state defined within the stratified layer, we then need to match to a Taylor state in the region beneath. One way of proceeding is to simply extend the polynomial description (already known) of the Malkus state beneath the stratified layer (where the solution

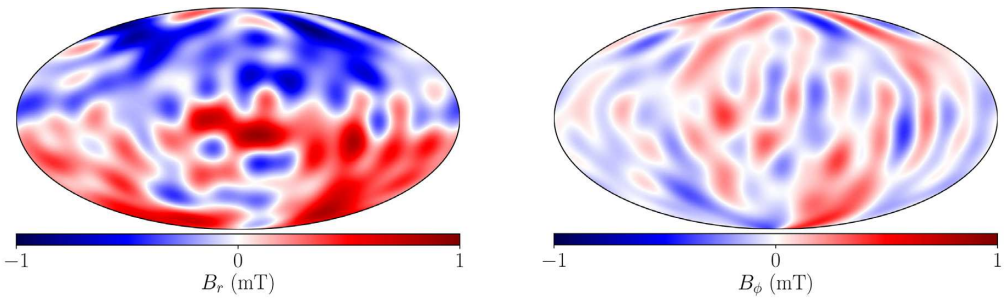

(a) B_r at the CMB, (max value = 0.91 mT). (b) B_ϕ at the CMB, (max value = 0.46 mT).

Figure 3. Magnetic field at the CMB based on the poloidal field fit to CHAOS-6 at epoch 2015. Visualized using the Mollweide projection and centred on the Greenwich meridian.

also satisfies Taylor constraint); however this effectively imposes additional constraints on the inner region and is overly restrictive. Instead, we apply a similar procedure as for the Malkus states to the inner solution: we use the same poloidal profile and expand the unknown toroidal field in the same way. Because the Taylor constraints are also now linear, this allows for an inner Taylor state to be found. This procedure can be applied to find a Malkus/Taylor state defined by any depth of stratification.

Even within these geomagnetically consistent Malkus states, there are nevertheless multiple degrees of freedom remaining. This raises the question of which of the multiple possible solutions are most realistic for the Earth, and motivates us to incorporate additional conditions to distinguish 'Earth-like' solutions.

We determine specific solutions through optimizing the toroidal field **T** either by its Ohmic dissipation or its energy, respectively

$$Q = \frac{\eta}{\mu_0}\int_V (\nabla \times \mathbf{T})^2 \mathrm{d}V, \qquad \mathcal{E} = \frac{1}{2\mu_0}\int_V \mathbf{T}^2 \mathrm{d}V,$$

where $\eta \approx 1$ m^{2}s^{-1} is magnetic diffusivity and $\mu_0 = 4\pi \times 10^{-7}$ NA^{-2} is the permeability of free space. Both of these target functions are quadratic in the magnetic field, and so seeking a minimal value subject to the now linear constraints is straightforward. In our sequential method to find a matched Malkus–Taylor state, we first optimize the Malkus state, and then subsequently find an optimal matching Taylor state.

Of the dissipation mechanisms in the core: Ohmic, thermal and viscous, the Ohmic losses are believed to dominate. On these grounds, the most efficient arrangement of the geomagnetic field would be such that Ohmic dissipation Q is minimized. It is worth noting that in general this procedure is not guaranteed to provide the Malkus state field with least dissipation, but only an approximation to it, since we effectively separately, rather than jointly, optimize for the poloidal and toroidal components. In terms of finding a Malkus state with minimum toroidal field energy, this is useful in allowing us to determine the weakest toroidal field which is required in order to transform the imposed poloidal field into a Malkus state.

6 EARTH-LIKE MALKUS STATES

We now present Malkus states found using the method explained above with minimal toroidal energy, applied to two external field models. First, we use the CHAOS-6 model (Finlay *et al.* 2016) at epoch 2015 evaluated to degree 13, the maximum obtainable from geomagnetic observations without significant interference due to crust magnetism (Kono 2015). Second, we use the time-averaged field over the last 10 000 yr from the CALS10k.2 model (Constable *et al.* 2016), which although is defined to degree 10 it has power concentrated mostly at degrees 1–4 because of strong regularization of sparsely observed ancient magnetic field structures. Recalling that the magnetostrophic state that we seek is defined over millennial timescales, this longer average provides on the one hand a better approximation to the background state, but on the other a much lower resolution.

The geometry assumed here is as illustrated in Fig. 1(a), with a Malkus state in the stratified layer in the region $0.9R < r \leq R$, matching to an inner Taylor state. The strength of the externally invisible but important toroidal field will be shown by contour plots of its azimuthal component. We note that the radial component of the magnetic field is defined everywhere by the imposed poloidal field of eq. (11).

6.1 Magnetic field at 2015

We begin by showing in Fig. 3 both the radial and azimuthal structure, B_r and B_ϕ, of the poloidal CHAOS-6 model at epoch 2015 on the CMB, $r = R$. Of note is that at the truncation to degree 13, the azimuthal component is about half as strong as the radial component.

Fig. 4 summarizes the strength of toroidal field as a function of radius, for different toroidal truncations $L_{\max} = N_{\max}$ (shown in different colours). The toroidal field is required to be four orders of magnitude stronger in the stratified layer in order to satisfy the more restrictive Malkus constraints, compared with the inner region in which the weaker Taylor constraint applies, and adopts a profile that is converged by degree 13. The strong toroidal field throughout the stratified layer occurs despite the electrically insulating boundary condition at the outer

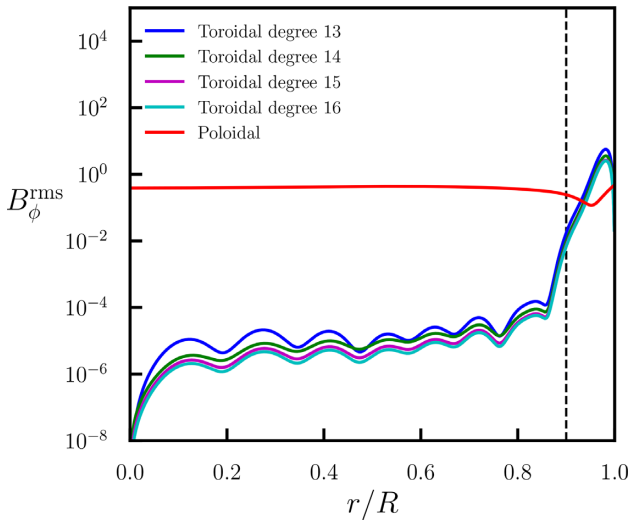

Figure 4. The rms azimuthal field strength (defined over solid angle) as a function of radius, comparing the strengths of the poloidal field (red) and toroidal field (blue, green, magneta and cyan) for toroidal fields with maximum spherical harmonic degree, order and radial resolution, 13–16, respectively. The poloidal field is the degree 13 field of minimum Ohmic dissipation compatible with the CHAOS-6 model at epoch 2015 (Finlay *et al.* 2016).

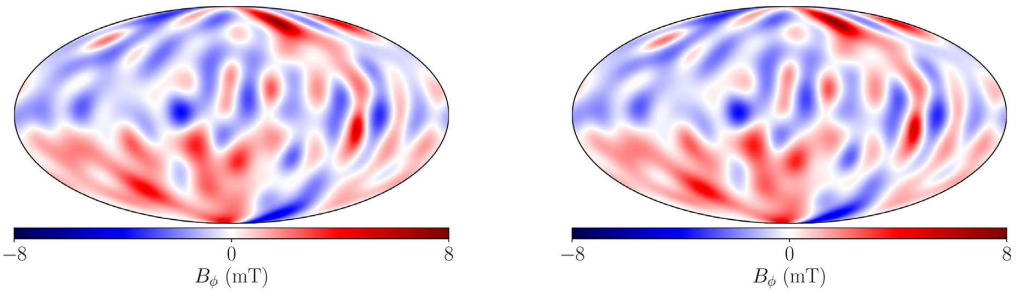

(a) Toroidal field B_ϕ at $r = 0.98R$, (max value = 7.74 mT, RMS = 2.50 mT).

(b) Total field B_ϕ at $r = 0.98R$, (max value = 7.80 mT, RMS = 2.53 mT).

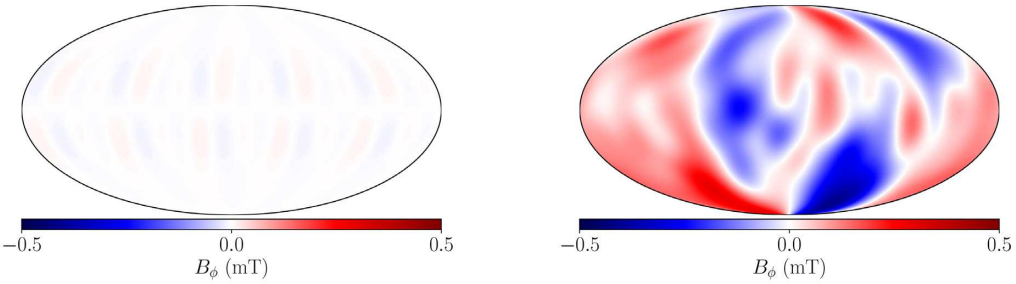

(c) Toroidal field B_ϕ at $r = 0.7R$, (max value = 0.012 mT)

(d) Total field B_ϕ at $r = 0.7R$, (max value = 0.41 mT)

Figure 5. Minimal toroidal-energy solution (a,c) shown by the azimuthal component, of a Malkus state ($0.9R < r \leq R$) and Taylor state $r \leq 0.9R$, compared with the total azimuthal component (b,d). Panels (a, b) show the field at a radius of $r = 0.98R$, close to where the maximum rms azimuthal toroidal field occurs, while (c, d) show the inner region at $r = 0.7R$.

boundary that requires the toroidal field to vanish. Within the stratified layer, the azimuthal toroidal field strength attains a maximum rms value of 2.5 mT at a radius of about $0.98R$ or a depth of about 70 km, about double the observed value at the CMB, and locally exceeds the imposed azimuthal poloidal magnetic field (of rms 0.28 mT at this radius).

Fig. 5 shows B_ϕ for both the total field and the toroidal component in isolation, using a toroidal truncation of 13 (corresponding to the blue line in Fig. 4.) The top row shows the structure at the radius of maximum rms toroidal field ($r = 0.98R$), demonstrating that the additive toroidal field component (of maximum 8 mT) dominates the total azimuthal field. The bottom row shows a comparable figure at $r = 0.7R$, in the inner region where only Taylor's constraint applies. Plotted on the same scale, the required additive toroidal component is tiny compared

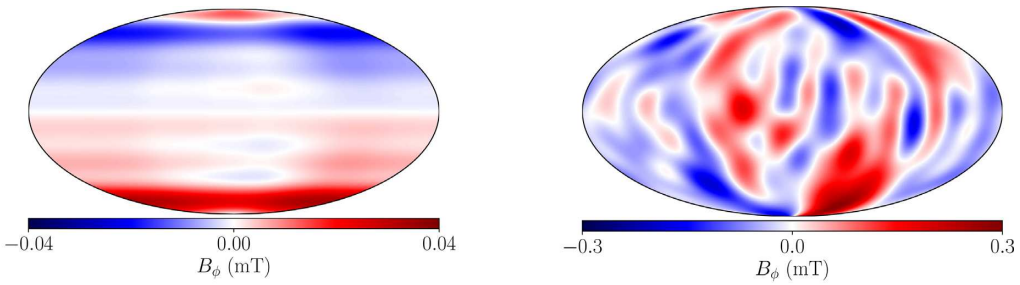

(a) Toroidal field B_ϕ at $r = 0.98R$, (max value = 0.034 mT)

(b) Total field B_ϕ at $r = 0.98R$, (max value = 0.29 mT)

Figure 6. Azimuthal field for an unstratified comparative case, for which the magnetic field satisfies only Taylor's constraint.

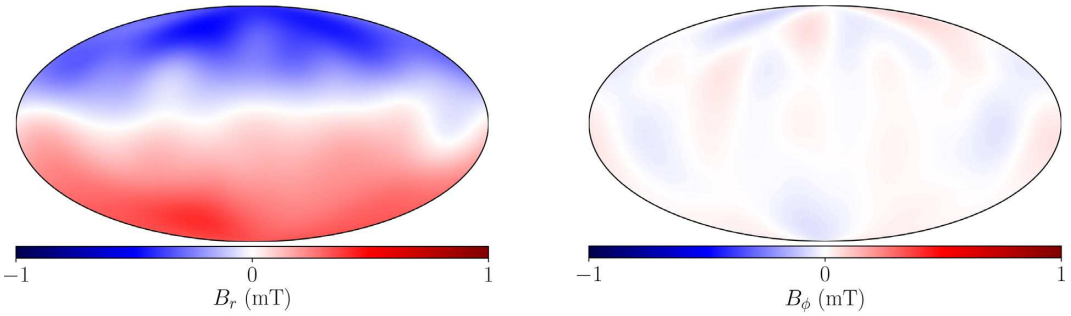

(a) B_r, max value = 0.50 mT.

(b) B_ϕ, max value = 0.085 mT.

Figure 7. Magnetic field at the CMB based on the 10 000-yr time average field from CALS10k.2.

with the imposed poloidal field. This results in a maximum value of the toroidal magnetic field within the outer layer which is about 100 times larger compared to that in the inner region. This highlights again that the Malkus constraint is much more restrictive than the Taylor constraint.

For comparison, Fig. 6 shows an equivalent solution to Figs 5(a) and (b) but in the absence of stratification (where the magnetic field satisfies only Taylor's constraint). The toroidal contribution to the azimuthal field is very weak (note the colourbar range is reduced from that of Figs 5a and b from 8 to 0.04 mT) and is of very large scale. This further highlights the weakness of the Taylor constraints compared with the Malkus constraints.

6.2 Time averaged field over the past ten millennia

Here we show results for a poloidal field that is derived from the 10 000-yr time averaged field from the CALS10k.2 model (Constable *et al.* 2016), which is as shown in Fig. 7. The model is only available up to spherical harmonic degree 10, hence we adopt a truncation of $L_{\max} = N_{\max} = 10$ for the toroidal field. Due to the absence of small-scale features in the field (caused by regularization) the maximum value of B_r is reduced to about 1/2 of the comparable value from the degree-13 CHAOS-6 model from epoch 2015, and similarly the azimuthal field to about 1/6 of its value. We note that over a long enough time span, Earth's magnetic field is generally assumed to average to an axial dipole: a field configuration that is both a Malkus state and one in which the azimuthal component vanishes. Thus a small azimuthal component is consistent with such an assumption.

Contours of the azimuthal field within the stratified layer (at $r = 0.97R$) are shown in Fig. 8, which is approximately the radius at which the maximum rms azimuthal toroidal field occurs. As before, the toroidal field dominates the azimuthal component whose rms (1.66 mT) is about 20 times that on the CMB (0.085 mT) and 4 orders of magnitude larger than in the interior core. Although its maximum absolute value is about 3 mT, less than the 8 mT found in the 2015 example above, this is consistent with the overall reduction in structure of the imposed poloidal field.

7 DISCUSSION

Having presented our results, we now begin our discussion by addressing in turn the three objectives listed at the beginning of the paper.

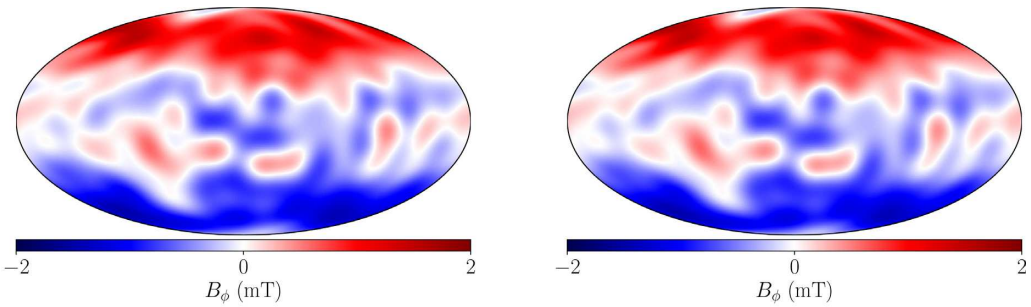

(a) Toroidal field B_ϕ at $r = 0.97R$, (max value = 1.60 mT)

(b) Total field B_ϕ at $r = 0.97R$, (max value = 1.66 mT)

Figure 8. The azimuthal component of the Malkus state magnetic field within the stratified layer at a radius of $r = 0.97R$, approximately the radius of maximum rms azimuthal toroidal field.

7.1 Do Malkus states exist?

We have shown that many exact Malkus states exist, both by imposing specific symmetries and by constructing states with a given poloidal field by solving linearly for a suitable toroidal field. We note that even within our linearized framework that ignores a significant part of the toroidal field, there are many such solutions. Owing to the non-linearity and the difficulty in enumerating the number of independent Malkus constraints, we have no way of quantifying the space of solutions, but it is surely large.

Moreover, the abundance of exact Malkus states also implies the existence of a plenitude of approximate Malkus states. These may indeed be more relevant for the Earth, where some of our idealized assumptions, for example an exact magnetostrophic force balance or zero radial flow, are relaxed.

7.2 Can we tell from a snapshot of the geomagnetic field if a stratified layer exists?

We have shown in this paper that any exterior potential field can be matched to a Malkus state. In fact our result is much stronger (see Appendix B), namely that we can fit a potential field to either a Taylor state (no stratification assumed), or a Malkus state (defined within a stratified layer of arbitrary depth). Thus if the core is in an exact magnetostrophic balance, then using only considerations of Malkus constraints means that instantaneous knowledge of the geomagnetic field outside the core cannot discriminate between the existence, or not, of a stratified layer.

However, incorporating considerations of the time-dependence of the geomagnetic field, from either a theoretical or observational perspective, may indeed provide additional information. For example, one might consider the evolution of a dynamo-generated time-dependent Malkus state, that satisfies all relevant constraints as time progresses. It is possible that examples of exterior fields are realized by the Earth that cannot match a time-dependent Malkus state. Furthermore, geomagnetic secular variation may provide an avenue to discriminate between observational signatures that are, or are not, compatible with a stratified layer: it may be that dynamics that are guided by stratification (such as waves) provide convincing evidence for such a layer, in a similar vein to the evidence from torsional waves (e.g. Gillet *et al.* 2010) which suggests that Earth's core is close to a Taylor state. Unfortunately a rigorous examination of the dynamics (and perturbations) of Malkus states is out of scope of this work.

7.3 What might be the present-day internal structure of the geomagnetic field inside a stratified layer?

Estimating the magnetic field strength inside the core is challenging, because observations made on Earth's surface, using a potential-field extrapolation, only constrain the poloidal magnetic structure down to the CMB and not beneath. Furthermore, even this structure is visible only to about spherical harmonic degree 13.

By constructing a Malkus state with minimal azimuthal field, we have estimated that for the modern (epoch 2015) field would achieve within the stratified layer (at radius $r = 0.98R$ or a depth of about 70 km) a maximum azimuthal component of around 8 mT. This value is consistent with other estimates of internal field strength that range between 1 and 100 mT (Zhang & Fearn 1993; Shimizu *et al.* 1998; Gubbins 2007; Buffett 2010; Gillet *et al.* 2010; Hori *et al.* 2015; Sreenivasan & Narasimhan 2017), relying on studies of numerical models, waves, electric field measurements, tides and reversed flux patches, which indicates that the assumptions underpinning our model are consistent with other approaches. Nevertheless, the strong toroidal field of 8 mT, about eight times stronger than the observed radial field of 1 mT on the CMB has significant implications for dynamics within the core. One important example is the speed of Magneto-Coriolis waves, which depends upon the average squared azimuthal field strength, as shown explicitly by Hori *et al.* (2015). Thus a stratified layer could support fast waves, for example the equatorial waves suggested by Finlay & Jackson (2003), driven in part by the stratification itself but possibly also by the stronger required magnetic field (Hori *et al.* 2018).

A key second result is that the azimuthal component of our solution within the inner unstratified region is about 100 times weaker than within the stratified layer. This demonstrates the extent to which Malkus' constraint is far more restrictive than Taylor's constraint, and requires a more complex and stronger magnetic field. If the Earth has a stratified layer, this suggests that the magnetic field within the layer would likely be quite different from that of the bulk of the core. This has profound implications on what can be inferred about deep-core dynamics such as large-scale flows (e.g. Holme 2015), since any inferences are based only on the magnetic field at the edge of the core, at the top of the layer. Indeed, if the magnetic field has a two layer structure, then the dynamics that it drives will also likely be different within each layer. The deeper dynamics would then be effectively screened from observation by the change in magnetic structure demanded by the stratified layer. Inverting this logic suggests that if deep core structures can be inferred by surface observations, that there can be no stratified layer. Relevant evidence for this line of argument comes from the close correspondence between changes in the length of day and the angular momentum carried by core flows, particularly between 1970 and 2000 (e.g. Barrois *et al.* 2017), although the link is not so well defined in the last few decades during the satellite era.

7.4 Limitations and robustness

Our model does not produce a formal lower bound on the azimuthal component of a magnetic field that satisfies both the Malkus and Taylor constraints in their relevant regions along with matching conditions at the CMB. Instead, our results give only an upper bound on the lower bound (e.g. Jackson *et al.* 2011) because we have made a variety of simplifying assumptions, the most notable of which are (i) we have restricted ourselves to a subspace of Malkus states for which the constraints are linear (ii) we have imposed the entire poloidal profile and (iii) we have used a regular basis set for all magnetic fields even within the stratified layer when this is not strictly necessary. However, we show for the example considered in Appendix A2 that in this case assumption (i) does not have a significant impact and our estimate is close to the full nonlinear lower bound. Also with regard to assumption (ii), we have experimented with some slightly different poloidal profiles, with the result being only small (less than 10%) variations in our azimuthal field estimates, indicating some generality of our results. It may be that the other assumptions also do not cause our azimuthal field estimates to deviate significantly from the actual lower bound.

There remains much uncertainty over the depth of any stably stratified layer at the top of the Earth's core (Hardy & Wong 2019). Hence it is natural to consider how our results may change if the layer were to be of a different thickness to the 10 % of core radius used, as such we also calculated minimum toroidal-energy solutions matched to CHAOS-6 in epoch 2015 for a range of layer thicknesses. We find very little dependence of the field strengths internal to the layer on the depth of the layer itself, with our root mean square azimuthal field taking peak values of 1.9, 2.7, 2.5, 2.4 and 2.1 mT for thicknesses of 1, 5, 10, 15 and 50 %, respectively. However for extremely thin layers such as a layer depth of 0.1%, the resulting peak is only of magnitude $B_\phi = 0.12$ mT and actually occurs beneath the stratified layer. This much smaller value is due to the immediate proximity of the boundary at which the toroidal field must vanish.

The resolution of poloidal field also impacts significantly our optimal solutions. This has already been identified in the comparison between the degree-13 2015 model, and the degree-10 10 000-yr time-averaged model, that respectively resulted in rms azimuthal field estimates of 2.5 and 1.2 mT. We can further test the effect of resolution by considering maximum poloidal degrees of 6 and 10 for the 2015 model to compare with our solution at degree 13. We find that our estimates for the root mean square azimuthal field (taken over their peak spherical surface) were 1.6 and 2.2 mT, respectively. In all these calculations, the spherical harmonic degree representing the toroidal field was taken high enough to ensure convergence. Thus stronger toroidal fields are apparently needed to convert more complex poloidal fields into a Malkus state. This has important implications for the Earth, for which we only know the degree of the poloidal field to about 13 due to crustal magnetism. Our estimates of the azimuthal field strength would likely increase if a full representation of the poloidal field were known.

7.5 Ohmic dissipation

Our method can be readily amended to minimize the toroidal Ohmic dissipation, rather than the toroidal energy. In so doing, we provide a new estimate of the lower bound of Ohmic dissipation within the core. Such lower bounds are useful geophysically as they are linked to the rate of entropy increase within the core, which has direct implications for: core evolution, the sustainability of the geodynamo, the age of the inner core and the heat flow into the mantle (Jackson *et al.* 2011).

The poloidal field with maximum spherical harmonic degree 13 that we use, based on CHAOS-6 (Finlay *et al.* 2016) and the minimum Ohmic dissipation radial profile (Backus *et al.* 1996) has by itself an Ohmic dissipation of 0.2 GW. Jackson & Livermore (2009) showed that by adding additional constraints for the magnetic field, a formal lower bound on the dissipation could be raised to 10 GW, and even higher to 100 GW with the addition of further assumptions about the geomagnetic spectrum. This latter bound is close to typical estimates of 1–15 TW (Jackson & Livermore 2009; Jackson *et al.* 2011).

The addition of extra conditions derived from the assumed dynamic balance, namely Taylor constraints, were considered by Jackson *et al.* (2011) by adopting a very specific magnetic field representation. These constraints alone raised their estimate of the lower bound from 0.2 to 10 GW, that is, by a factor of 50. In view of the much stronger Malkus constraints (compared to the Taylor constraints), we briefly investigate their impact here.

We follow our methodology and find an additive toroidal field of minimal dissipation (rather than energy) that renders the total field a Malkus state. The dissipation is altered from 0.2 to 0.7 GW. That this increase is rather small (only a small factor of about 3) is rather disappointing, but is not in contradiction to our other results. It is generally true that the Malkus constraints are more restrictive than the Taylor constraint, but this comparison can only be made when the same representation is used for both. The method of Jackson *et al.* (2011) assumed a highly restrictive form, so that in fact their Taylor states were apparently actually more tightly constrained than our Malkus states and thus produced a higher estimate of the lower bound. Despite our low estimate here, additional considerations of the Malkus constraints may increase the highest estimates of Jackson & Livermore (2009) well into the geophysically interesting regime.

7.6 Further extensions

The Malkus states we have computed, which match to exterior potential fields, provide a plausible background state at the top of the core. It may be interesting for future work to investigate how waves thought to exist within such a stratified layer (e.g. Buffett 2014) may behave when considered as perturbations from such a background state, and whether they remain compatible with the observed secular variation in the geomagnetic field. Similarly, combining our analysis with constraints on B_s from torsional wave models (Gillet *et al.* 2010) may be insightful, and would combine aspects of both long and short-term dynamics.

It is worth noting though, that we have investigated only static Malkus states without consideration of dynamics: we do not require the magnetic field to be either steady or stable, both of which would apply additional important conditions. An obvious extension to this work then is to investigate the fluid flows which are generated by the Lorentz force associated with these magnetic fields. This would then allow a consideration of how such flows would modify the field through the induction equation. These dynamics are however still relatively poorly known even for the much simpler problem of Taylor states. Recent progress by Hardy *et al.* (2018) now allows a full calculation of the flow driven by a Taylor state. A general way to discover stationary and stable Taylor states comparable with geomagnetic observations is still out of reach, and currently the only way to find a stable Taylor state is by time-stepping (e.g. Li *et al.* 2018).

The well established test used to determine whether the appropriate magnetostrophic force balance is achieved within numerical dynamo simulations is 'Taylorization', which represents a normalized measure of the magnitude of the Taylor integral eq. (2) and hence the departure from the geophysically relevant, magnetostrophic regime (e.g. Takahashi *et al.* 2005).

We propose an analogous quantity termed 'Malkusization' defined in the same way, in terms of the Malkus integral:

$$\text{Malkusization} = \frac{\left| \int_0^{2\pi} ([\nabla \times \mathbf{B}] \times \mathbf{B})_\phi \mathrm{d}\phi \right|}{\int_0^{2\pi} |([\nabla \times \mathbf{B}] \times \mathbf{B})_\phi| \mathrm{d}\phi}.$$

This quantity is expected to be very small within a stratified layer adjacent to a magnetostrophic dynamo, provided stratification is sufficiently strong. The recently developed dynamo simulations of Christensen (2018), Olson *et al.* (2018) and Gastine *et al.* (2019), which incorporate the presence of a stratified layer can utilize the computation of this quantity to access the simulation regime. Additionally, magnetic fields from these dynamo simulations could be incorporated into our modelling, through providing a poloidal field to a resolution beyond the degree 13 exterior potential field. It would be interesting to discover how these may change the resultant bound on the required toroidal field and how this value compares to both that within the simulation and indeed the existing estimates for the Earth.

Finally, we note that the appropriate description of a stratified layer may in fact need to be more complex than a single uniform layer that we assume. Numerical simulations of core flow with heterogeneous CMB heat flux by Mound *et al.* (2019) find that localized subadiabatic regions that are stratified are possible amid the remaining actively convecting liquid. If indeed local rather than global stratification is the more appropriate model for the Earth's outermost core then the condition of requiring an exact Malkus state would not apply, and the constraints on the magnetic field would be weakened by the existence of regions of non-zero radial flow.

8 CONCLUSION

In this paper, we have shown how to construct magnetic fields that are consistent with a strongly stratified layer and the exact magnetostrophic balance thought to exist within Earth's core. We have found that these *Malkus states* are abundant, so much so that one can always be found that matches any exterior potential field (for example as derived from observational geomagnetic data).

However, despite this, the Malkus constraints derived here are proven to be significantly more restrictive than the equivalent conditions within an unstratified fluid, those of the well known Taylor constraints. The structure of magnetic fields that satisfy the Malkus constraints gives insight into the nature of the Earth's magnetic field immediately beneath the CMB, where a layer of stratified fluid may be present. We find that the increased restrictions in the constraints requires an enhanced magnetic field within the layer. We estimate that for the present-day, the toroidal field within the stratified layer is about 8 mT. This suggests that the stratified layer may be distinct from the inner convective part of the core, characterized not only by suppressed radial flow but by a strong magnetic field, and may support different dynamics to those of the bulk of the core.

ACKNOWLEDGEMENTS

This work was supported by the Engineering and Physical Sciences Research Council (EPSRC) Centre for Doctoral Training in Fluid Dynamics at the University of Leeds under Grant No. EP/L01615X/1. P.W.L. acknowledges partial support from NERC grant NE/G014043/1. The authors would also like to thank Dominique Jault and Emmanuel Dormy for helpful discussions, the Leeds Deep Earth group for useful comments, as well as Richard Holme and an anonymous reviewer for feedback that led to an improved manuscript. Figures were produced using matplotlib (Hunter 2007).

REFERENCES

Alexandrakis, C. & Eaton, D., 2010. Precise seismic-wave velocity atop Earth's core: no evidence for outer-core stratification, *Phys. Earth planet. Inter.,* **180**(1), 59–65.

Amit, H., 2014. Can downwelling at the top of the Earth's core be detected in the geomagnetic secular variation?, *Phys. Earth planet. Inter.,* **229**(C), 110–121.

Aubert, J., 2012. Flow throughout the earth's core inverted from geomagnetic observations and numerical dynamo models, *Geophys. J. Int.,* **192**(2), 537–556.

Aubert, J., 2014. Earth's core internal dynamics 1840–2010 imaged by inverse geodynamo modelling, *Geophys. J. Int.,* **197**(3), 1321–1334.

Aubert, J., 2019. Approaching Earth's core conditions in high-resolution geodynamo simulations, *Geophys. J. Int.,* **219**(Suppl. 1), S137–S151.

Aubert, J. & Finlay, C., 2019. Geomagnetic jerks and rapid hydromagnetic waves focusing at Earth's core surface, *Nat. Geosci.,* **12**(5), 393.

Aubert, J. & Fournier, A., 2011. Inferring internal properties of earth's core dynamics and their evolution from surface observations and a numerical geodynamo model, *Nonlin. Proc. Geophys.,* **18**(5), 657–674.

Backus, G., Parker, R. & Constable, C., 1996. *Foundations of Geomagnetism,* Cambridge Univ. Press.

Barrois, O., Gillet, N. & Aubert, J., 2017. Contributions to the geomagnetic secular variation from a reanalysis of core surface dynamics, *Geophys. J. Int.,* **211**(1), 50–68.

Bouffard, M., Choblet, G., Labrosse, S. & Wicht, J., 2019. Chemical convection and stratification in the Earth's outer core, *Front. Earth Sci.,* **7,** 99.

Braginsky, S., 1967. Magnetic waves in the Earth's core, *Geomagnet. Aeron.,* **7,** 851–859.

Braginsky, S., 1987. Waves in a stably stratified layer on the surface of the terrestrial core, *Geomagn. Aeron.,* **27,** 410–414.

Braginsky, S., 1993. Mac-oscillations of the hidden ocean of the core, *J. Geomag. Geoelectr.,* **45**(11-12), 1517–1538.

Braginsky, S., 1999. Dynamics of the stably stratified ocean at the top of the core, *Phys. Earth planet. Inter.,* **111**(1), 21–34.

Braginsky, S., 2006. Formation of the stratified ocean of the core, *Earth planet. Sci. Lett.,* **243**(3–4), 650–656.

Buffett, B., 2010. Tidal dissipation and the strength of the Earth's internal magnetic field, *Nature,* **468**(7326), 952–954.

Buffett, B., 2014. Geomagnetic fluctuations reveal stable stratification at the top of the Earth's core, *Nature,* **507**(7493), 484–487.

Buffett, B. & Seagle, C., 2010. Stratification of the top of the core due to chemical interactions with the mantle, *J. geophys. Res.,* **115**(B4), doi:10.1029/2009JB006751.

Buffett, B., Knezek, N. & Holme, R., 2016. Evidence for mac waves at the top of Earth's core and implications for variations in length of day, *Geophys. J. Int.,* **204**(3), 1789–1800.

Busse, F.H., 1975. A necessary condition for the Geodynamo, *J. geophys. Res.,* **80,** 278–280.

Christensen, U., 2018. Geodynamo models with a stable layer and heterogeneous heat flow at the top of the core, *Geophys. J. Int.,* **215**(2), 1338–1351.

Christensen, U. & Wicht, J., 2008. Models of magnetic field generation in partly stable planetary cores: applications to Mercury and Saturn, *Icarus,* **196**(1), 16–34.

Christensen, U. & Wicht, J., 2015. Numerical dynamo simulations, in *Core Dynamics. Treatise on Geophysics*, Vol. 8, pp. 245–277, ed. Olson P., Elsevier.

Christensen, U., Holzwarth, V. & Reiners, A., 2009. Energy flux determines magnetic field strength of planets and stars, *Nature,* **457**(7226), 167.

Christensen, U., Aubert, J. & Hulot, G., 2010. Conditions for Earth-like geodynamo models, *Earth planet. Sci. Lett.,* **296**(3-4), 487–496.

Constable, C., Korte, M. & Panovska, S., 2016. Persistent high paleosecular variation activity in southern hemisphere for at least 10 000 years, *Earth planet. Sci. Lett.,* **453,** 78–86.

Cox, G., Davies, C., Livermore, P. & Singleton, J., 2019. Penetration of boundary-driven flows into a rotating spherical thermally stratified fluid, *J. Fluid Mech.,* **864,** 519–553.

Davies, C., Pozzo, M., Gubbins, D. & Alfè, D., 2015. Constraints from material properties on the dynamics and evolution of Earth's core, *Nat. Geosci.,* **8**(9), 678–685.

Fearn, D., 1998. Hydromagnetic flow in planetary cores, *Rep. Prog. Phys.,* **61,** 175–235.

Finlay, C. & Jackson, A., 2003. Equatorially dominated magnetic field change at the surface of Earth's core, *Science,* **300**(5628), 2084–2086.

Finlay, C., Olsen, N., Kotsiaros, S., Gillet, N. & Toeffner-Clausen, L., 2016. Recent geomagnetic secular variation from *Swarm* and ground observatories as estimated in the CHAOS-6 geomagnetic field model, *Earth Planets Space,* **68**(1), 1–18.

Fournier, A., Eymin, C. & Alboussiere, T., 2007. A case for variational geomagnetic data assimilation: insights from a one-dimensional, nonlinear, and sparsely observed MHD system, *Nonlin. Proc. Geophys.,* **14,** 163–180.

Gastine, T., Aubert, J. & Fournier, A., 2019. Dynamo-based limit to the extent of a stable layer atop Earth's core, *Geophys. J. Int.,* **222,** 2, 1433–1448, doi:10.1093/gji/ggaa250.

Gillet, N., Jault, D., Canet, E. & Fournier, A., 2010. Fast torsional waves and strong magnetic field within the Earth's core, *Nature,* **465**(7294), 74–77.

Glane, S. & Buffett, B., 2018. Enhanced core-mantle coupling due to stratification at the top of the core, *Front. Earth Sci. ,* **6,** 171, doi:10.3389/feart.2018.00171.

Gross, R., 2001. A combined length-of-day series spanning 1832–1997: Lunar97, *Phys. Earth planet. Inter.,* **123**(1), 65–76.

Gubbins, D., 2007. Geomagnetic constraints on stratification at the top of Earth's core, *Earth, Planets Space,* **59**(7), 661–664.

Hardy, C. & Wong, J., 2019. Stably stratified layers within Earth's core, *Astron. Geophys.,* **60**(3), 3–30.

Hardy, C., Livermore, P., Niesen, J., Luo, J. & Li, K., 2018. Determination of the instantaneous geostrophic flow within the three-dimensional magnetostrophic regime, *Proc. R. Soc. A,* **474**(2218), 20180412.

Helffrich, G. & Kaneshima, S., 2010. Outer-core compositional stratification from observed core wave speed profiles, *Nature,* **468**(7325), 807–810.

Helffrich, G. & Kaneshima, S., 2013. Causes and consequences of outer core stratification, *Phys. Earth planet. Inter.,* **223,** 2–7.

Hollerbach, R. & Ierley, G., 1991. A modal α^2-dynamo in the limit of asymptotically small viscosity, *Geophys. Astrophys. Fluid Dyn.,* **56,** 133–158.

Holme, R., 2015. Large-scale flow in the core, *Treat. Geophys.,* **8,** 91–113.

Holme, R. & De Viron, O., 2005. Geomagnetic jerks and a high-resolution length-of-day profile for core studies, *Geophys. J. Int.,* **160**(2), 435–439.

Hori, K., Jones, C. & Teed, R., 2015. Slow magnetic Rossby waves in the Earth's core, *Geophys. Res. Lett.,* **42**(16), 6622–6629.

Hori, K., Teed, R. & Jones, C., 2018. The dynamics of magnetic Rossby waves in spherical dynamo simulations: a signature of strong-field dynamos?, *Phys. Earth planet. Inter.,* **276,** 68–85.

Hunter, J., 2007. Matplotlib: a 2D graphics environment, *Comp. Sci. Eng.,* **9**(3), 90–95.

Irving, J., Cottaar, S. & Lekić, V., 2018. Seismically determined elastic parameters for Earth's outer core, *Sci. Adv.,* **4**(6), eaar2538, doi:10.1126/sciadv.aar2538.

Jackson, A. & Finlay, C., 2015. Geomagnetic secular variation and its applications to the core, *Treat. Geophys.*, **5,** 137–184.
Jackson, A. & Livermore, P., 2009. On Ohmic heating in the Earth's core. I: nutation constraints, *Geophys. J. Int.,* **179**(2), 923–928.
Jackson, A., Livermore, P. & Ierley, G., 2011. On ohmic heating in the Earth's core. II: poloidal magnetic fields obeying taylor's constraint, *Phys. Earth planet. Inter.,* **187**(3-4), 322–327.
Jault, D. & Cardin, P., 1999. On dynamic geodynamo models with imposed velocity as energy source, *Phys. Earth Planet. Int.,* **111,** 75–81.
Jeanloz, R., 1990. The nature of the Earth's core, *Ann. Rev. Earth Planet. Sci.,* **18**(1), 357–386.
Kaneshima, S., 2017. Array analyses of SmKS waves and the stratification of earth's outermost core, *Phys. Earth planet. Inter.,* **276,** 234–246.
Kono, M., 2015. Geomagnetismμan introduction and overview, *Treat. Geophys.,* **5,** 1–30.
Lay, T. & Young, C., 1990. The stably-stratified outermost core revisited, *Geophys. Res. Lett.,* **17**(11), 2001–2004.
Lesur, V., Whaler, K. & Wardinski, I., 2015. Are geomagnetic data consistent with stably stratified flow at the core-mantle boundary?, *Geophys. J. Int.,* **201**(2), 929–946.
Lewis, H. & Bellan, P., 1990. Physical constraints on the coefficients of Fourier expansions in cylindrical coordinates, *J. Math. Phys.,* **31**(11), 2592–2596.
Li, K., Livermore, P.W. & Jackson, A., 2010. An optimal Galerkin scheme to solve the kinematic dynamo eigenvalue problem in a full sphere, *J. Comput. Phys.,* **229**(23), 8666–8683.
Li, K., Jackson, A. & Livermore, P., 2011. Variational data assimilation for the initial value dynamo problem, *Phys. Rev. E,* **84**(5), 056321.
Li, K., Jackson, A. & Livermore, P., 2018. Taylor state dynamos found by optimal control: axisymmetric examples, *J. Fluid Mech.,* **853,** 647–697.
Livermore, P. & Hollerbach, R., 2012. Successive elimination of shear layers by a hierarchy of constraints in inviscid spherical-shell flows, *J. Math. Phys.,* **53**(7), 073104.
Livermore, P., Ierley, G. & Jackson, A., 2008. The structure of Taylor's constraint in three dimensions, *Proc. R. Soc. Lond., A,* **464,** 3149–317.
Livermore, P., Ierley, G. & Jackson, A., 2009. The construction of exact Taylor states. I: the full sphere, *Geophys. J. Int.,* **179**(2), 923–928.
Malkus, W., 1967. Hydromagnetic planetary waves, *J. Fluid Mech.,* **28**(4), 793–802.
Malkus, W., 1979. Dynamo macrodynamics in rotating stratified fluids, *Phys. Earth planet. Inter.,* **20**(2-4), 181–184.
Mound, J., Davies, C., Rost, S. & Aurnou, J., 2019. Regional stratification at the top of Earth's core due to core-mantle boundary heat flux variations, *Nat. Geosci.,* **12,** 575–580.
Nakagawa, T., 2011. Effect of a stably stratified layer near the outer boundary in numerical simulations of a magnetohydrodynamic dynamo in a rotating spherical shell and its implications for earth's core, *Phys. Earth planet. Inter.,* **187**(3-4), 342–352.
Olson, P., Landeau, M. & Reynolds, E., 2017. Dynamo tests for stratification below the core-mantle boundary, *Phys. Earth planet. Inter.,* **271,** 1–18.
Olson, P., Landeau, M. & Reynolds, E., 2018. Outer core stratification from the high latitude structure of the geomagnetic field, *Front. Earth Sci.,* **6,** 140.
Pozzo, M., Davies, C., Gubbins, D. & Alfè, D., 2012. Thermal and electrical conductivity of iron at Earth's core conditions, *Nature,* **485,** 355–358.
Roberts, P. & Aurnou, J., 2011. On the theory of core-mantle coupling, *Geophys. Astrophys. Fluid. Dyn.,* **106**(2), 157–230.
Roberts, P. & Wu, C., 2014. On the modified Taylor constraint, *Geophys. Astrophys. Fluid Dyn.,* **108**(6), 696–715.
Roberts, P. & Wu, C., 2018. On magnetostrophic mean-field solutions of the geodynamo equations. Part 2, *J. Plasma Phys.,* **84**(4), doi:10.1017/S0022377818000545.
Roberts, P. & Wu, C., 2020. On magnetostrophic dynamos in annular cores, *Geophys. Astrophys. Fluid Dyn.,* 1–53.
Roberts, P., Yu, Z. & Russell, C., 2007. On the 60-year signal from the core, *Geophys. Astrophys. Fluid. Dyn.,* **101**(1), 11–35.
Schaeffer, N., Jault, D., Nataf, H.C. & Fournier, A., 2017. Turbulent geodynamo simulations: a leap towards Earth's core, *Geophys. J. Int.,* **211**(), 1–29.
Shimizu, H., Koyama, T. & Utada, H., 1998. An observational constraint on the strength of the toroidal magnetic field at the CMB by time variation of submarine cable voltages, *Geophys. Res. Lett.,* **25**(21), 4023–4026.
Soward, A. & Jones, C., 1983. α^2-Dynamos and Taylor's constraint, *Geophys. Astrophys. Fluid Dyn.,* **27,** 87–122.
Sprain, C., Biggin, A., Davies, C., Bono, R. & Meduri, D., 2019. An assessment of long duration geodynamo simulations using new paleomagnetic modeling criteria (QPM), *Earth planet. Sci. Lett.,* **526,** 115758.
Sreenivasan, B. & Narasimhan, G., 2017. Damping of magnetohydrodynamic waves in a rotating fluid, *J. Fluid Mech.,* **828,** 867–905.
Stanley, S. & Mohammadi, A., 2008. Effects of an outer thin stably stratified layer on planetary dynamos, *Phys. Earth planet. Inter.,* **168**(3-4), 179–190.
Takahashi, F., Matsushima, M. & Honkura, Y., 2005. Simulations of a quasi-Taylor state geomagnetic field including polarity reversals on the earth simulator, *Science,* **309,** 459–461.
Taylor, J., 1963. The magneto-hydrodynamics of a rotating fluid and the Earth's dynamo problem, *Proc. R. Soc. A,* **9,** 274–283.
Whaler, K., 1980. Does the whole of the earth's core convect?, *Nature,* **287**(5782), 528.
Wicht, J. & Christensen, U., 2010. Torsional oscillations in dynamo simulations, *Geophys. J. Int.,* **181,** 1367–1380.
Wicht, J. & Sanchez, S., 2019. Advances in geodynamo modelling, *Geophys. Astrophys. Fluid Dyn.,* **113**(1-2), 2–50.
Wu, C. & Roberts, P., 2015. On magnetostrophic mean-field solutions of the geodynamo equations, *Geophys. Astrophys. Fluid Dyn.,* **109**(1), 84–110.
Yan, C. & Stanley, S., 2018. Sensitivity of the geomagnetic octupole to a stably stratified layer in the earth's core, *Geophys. Res. Lett.,* **45**(20), 11–005.
Zhang, K. & Fearn, D.R., 1993. How strong is the invisible component of the magnetic field in the Earth's core, *Geophys. Res. Lett.,* **20**(19), 2083–2086.

APPENDIX A: FULL SPHERE MALKUS STATES

A1 Simple example

Here we consider a simple example of an axisymmetric magnetic field in a full sphere of radius R, consisting of four modes: a toroidal $l = 1$, $n = 1$ mode, a toroidal $l = 1$, $n = 2$ mode, a poloidal $l = 1$, $n = 1$ mode and a poloidal $l = 1$, $n = 2$ mode, each of which has an unspecified corresponding coefficient $\alpha_{l,n}$ and $\beta_{l,n}$ for toroidal and poloidal modes, respectively. Through this we demonstrate the form of the linear constraints which arise from Malkus' constraint in this case. It is significant to note the vital role of degeneracy within these constraints in permitting a solution.

Through computing the Malkus integral and enforcing that this is zero for all values of s and z by requiring that the coefficients of all powers of s and z vanish we obtain a series of simultaneous equations:

$$\left(-\frac{11}{8}\beta_{1,2} + 2\beta_{1,1}\right)\alpha_{1,2} - \frac{253}{140}\left(\frac{77}{69}\beta_{1,2} + \frac{56}{759}\beta_{1,1}\right)\alpha_{1,1} = 0,$$

$$\left(\frac{319}{84}\beta_{1,2} - \frac{10}{3}\beta_{1,1}\right)\alpha_{1,2} - \frac{253}{70}\beta_{1,2}\alpha_{1,1} = 0,$$
$$\left(-\frac{165}{56}\beta_{1,2} + \beta_{1,1}\right)\alpha_{1,2} - \frac{253}{140}\beta_{1,2}\alpha_{1,1} = 0,$$
$$\left(\frac{319}{84}\beta_{1,2} - \frac{10}{3}\beta_{1,1}\right)\alpha_{1,2} - \frac{253}{70}\beta_{1,2}\alpha_{1,1} = 0,$$
$$\left(-\frac{165}{28}\beta_{1,2} + 2\beta_{1,1}\right)\alpha_{1,2} - \frac{253}{70}\beta_{1,2}\alpha_{1,1} = 0,$$
$$\left(-\frac{165}{56}\beta_{1,2} + \beta_{1,1}\right)\alpha_{1,2} - \frac{253}{140}\beta_{1,2}\alpha_{1,1} = 0.$$

Although there are six equations here, there are only two independent conditions:

$$\alpha_{1,1}\beta_{1,2} + \frac{5}{2}\alpha_{1,2}\beta_{1,2} = 0, \quad \text{and} \quad \alpha_{1,2}\beta_{1,1} + \frac{11}{7}\alpha_{1,2}\beta_{1,2} = 0.$$

If both $\beta_{1,2}$ and $\alpha_{1,2}$ are non-zero, then these become linear constraints.

Hence, in this case we can see that there are 4 degrees of freedom, 6 constraint equations but only 2 independent constraints. This means that while on first inspection the system appears to be overconstrained with no solution, there are in fact multiple Malkus state solutions, with the solution space being spanned by two degrees of freedom ($\beta_{1,2}$, $\alpha_{1,2}$) with the other coefficients determined in terms of these by the relationships:

$$\alpha_{1,1} = -\frac{5}{2}\alpha_{1,2} \quad \text{and} \quad \beta_{1,1} = -\frac{11}{7}\beta_{1,2}.$$

Despite the significant degeneracy in the Malkus constraints, they are notably more restrictive than the Taylor constraints for this truncation of $L_{\max} = 1$, $N_{\max} = 2$, for which the Taylor integral is identically zero and so provides no restriction.

A2 Solution of a low-resolution system

We now present a simple non-trivial solution of a Malkus state, without making any simplifying assumptions as to the form of the toroidal field. Here we consider a full sphere magnetic field truncated at $L_{\max} = 3$, $N_{\max} = 3$, and impose a minimum Ohmic dissipation poloidal profile that matches the CHAOS-6 model (to degree 3) at $r = R$. We seek a toroidal field using all spherical harmonic modes within the truncation $L_{\max} = 3$, $N_{\max} = 3$ (described by 45 degrees of freedom) that when added to this poloidal field satisfies the Malkus constraints. Of the 72 non-linear constraint equations, only 42 are independent. Thus the number of degrees of freedom exceed the number of independent constraints, although since the constraints are non-linear it is not immediate that a solution exists. However, using the computer algebra software Maple, we find the solution that minimizes toroidal field strength as well as satisfying all the constraints, which is visualized in Fig. A1. We cannot generalize this procedure to higher resolutions because of the numerical difficulty in finding optimal solutions in such a non-linear problem.

For comparison (see Fig. A2) we also compute the solution using the method described in Section 5, which owing to the specific choice of toroidal spherical harmonic modes results in a linear system. The solutions are qualitatively and quantitatively similar, with rms values of B_ϕ of 0.21 and 0.23 mT for the non-linear and linear solutions, respectively, suggesting that the optimized linear solutions we have found are close to those optimal solution based on the full non-linear system.

APPENDIX B: A SPECIAL CLASS OF MALKUS STATES

Theorem 1. Any arbitrary, prescribed, polynomial poloidal field can be transformed into a Malkus state through the addition of an appropriate polynomial toroidal field.

Proof. We prove below that by considering an arbitrary, prescribed, truncated polynomial poloidal field, the addition of a specific choice of toroidal modes renders the Malkus constraints linear in the unknown toroidal coefficients. By taking a sufficient number of such modes such that the degrees of freedom exceed the number of constraints, it follows that for the general case (barring specific degenerate cases) by solving the linear system the resultant magnetic field is a Malkus state.

To show this, because the Malkus constraint is quadratic in the magnetic field, we introduce the concept of a magnetic field interaction. In general there are three possible field interactions within the Malkus integral, toroidal–toroidal, poloidal–poloidal and toroidal–poloidal, respectively

$$M = \sum_{l_1,l_2}^{L_{max}} \sum_{m}^{L_{max}} \left([\boldsymbol{T}_{l_1}^m, \boldsymbol{T}_{l_2}^m] + [\boldsymbol{S}_{l_1}^m, \boldsymbol{S}_{l_2}^m] + [\boldsymbol{T}_{l_1}^m, \boldsymbol{S}_{l_2}^m] \right)$$

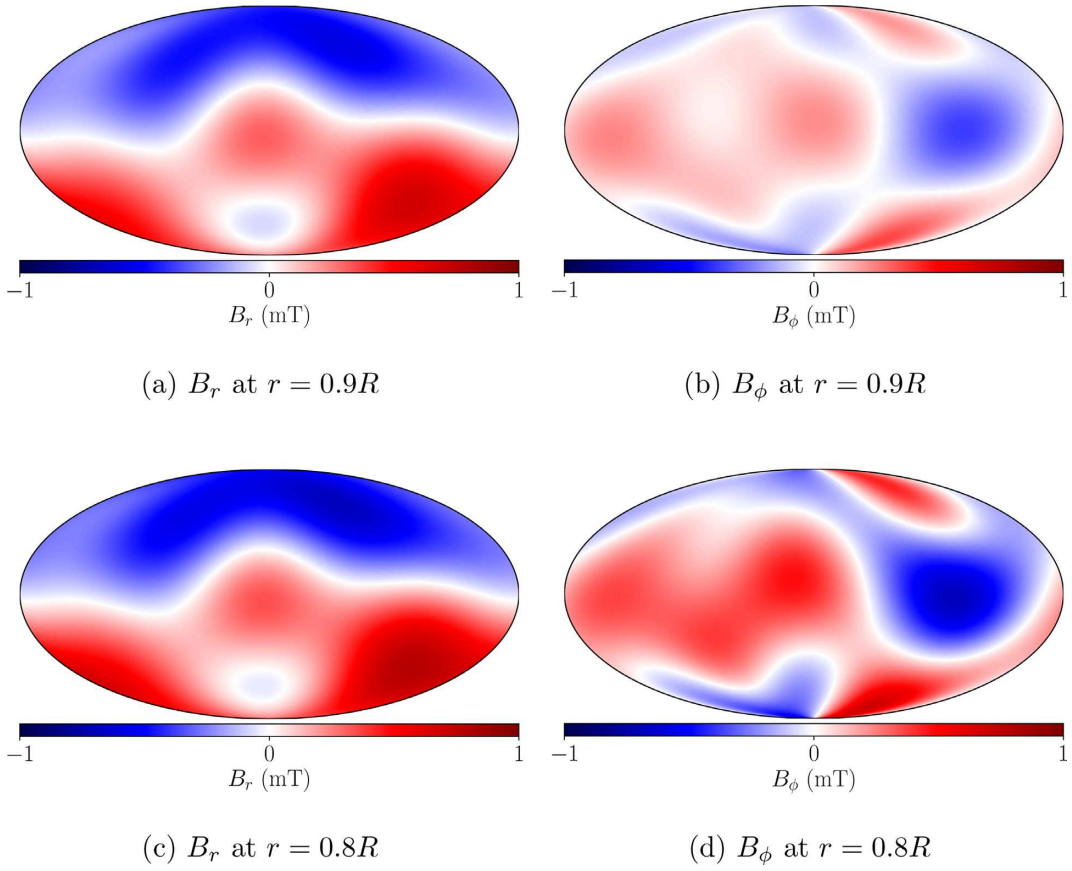

Figure A1. Fully non-linear Malkus state with $L_{\max} = 3$, $N_{\max} = 3$ with minimal toroidal field.

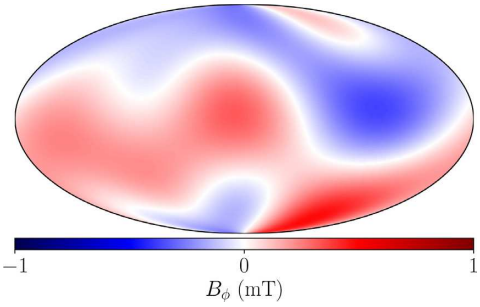

Figure A2. Linear Malkus state with minimal toroidal field, showing B_ϕ at $r = 0.9R$, using the method outlined in Section 5 and used for the Earth-like solutions.

where

$$[\boldsymbol{T}^m_{l_l}, \boldsymbol{T}^m_{l_2}] = \int_0^{2\pi} \frac{l_1(l_1+1)\mathcal{T}^m_{l_l}\mathcal{T}^m_{l_2}}{r^3 \sin\theta}\left(Y^m_{l_l}\frac{\partial Y^m_{l_2}}{\partial \phi}\right) s \, \mathrm{d}\phi + sc,$$

$$[\boldsymbol{S}^m_{l_l}, \boldsymbol{S}^m_{l_2}] = \int_0^{2\pi} \frac{l_1(l_1+1)\mathcal{S}^m_{l_l}(\frac{\mathrm{d}^2}{\mathrm{d}r^2} - l_2(l_2+1)/r^2)\mathcal{S}^m_{l_2}}{r^3 \sin\theta}\left(Y^m_{l_l}\frac{\partial Y^m_{l_2}}{\partial \phi}\right) s \, \mathrm{d}\phi + sc,$$

$$[\boldsymbol{T}^m_{l_l}, \boldsymbol{S}^m_{l_2}] = \int_0^{2\pi} \frac{1}{r^3}\left(l_1(l_1+1)T^m_{l_l}\frac{\mathrm{d}\mathcal{S}^m_{l_2}}{\mathrm{d}r}Y^m_{l_1}\frac{\partial Y^m_{l_2}}{\partial \theta} - l_2(l_2+1)\mathcal{S}^m_{l_2}\frac{\mathrm{d}T^m_{l_1}}{\mathrm{d}r}Y^m_{l_2}\frac{\partial Y^m_{l_1}}{\partial \theta}\right) s \, \mathrm{d}\phi, \tag{B1}$$

where sc is the symmetric counterpart given by interchanging the vector harmonics and hence the positions of l_1 and l_2 (Livermore *et al.* 2008). Note that there is no poloidal–toroidal interaction since the curl of a poloidal vector is toroidal and $(\boldsymbol{\mathcal{T}_1} \times \boldsymbol{\mathcal{T}_2})_\phi = 0$, for any two toroidal vectors $\boldsymbol{\mathcal{T}_1}$ and $\boldsymbol{\mathcal{T}_2}$.

For the situation we consider of a given poloidal field, then the only non-linearity within the unspecified coefficients arises from the toroidal–toroidal interactions, which results in quadratic dependence, just as for the general case with unprescribed poloidal field. However, by restricting attention to toroidal fields that result in no toroidal–toroidal interaction, the unknown toroidal coefficients appear only in a linear

form through the toroidal–poloidal interactions. Axisymmetric modes are the simplest set of toroidal modes which are non-self-interacting, however there are too few of them (within the truncation) to solve the resulting linear system which is overconstrained (see Fig. 2).

Therefore we require additional non-axisymmetric toroidal modes, which we choose such that the total set of toroidal modes remains non-self-interacting. This is achieved by exploiting the previously noted observations that any single harmonic is a Malkus state and that the set of equatorially symmetric toroidal modes T_l^l is a Malkus state (and therefore has no self-interaction). Owing additionally to azimuthal symmetry, the modes

$$T_1^0, T_2^0, \cdots, T_1^{-1}, T_1^1, T_2^{-2}, T_2^2, \ldots,$$

that is, the modes T_l^m with $m = 0$ or $m = \pm l$, have no self-interactions. Each harmonic mode may be expanded in radial modes up to the truncation $N_{\max}$. The non-interacting nature of the modes may be confirmed from eq. (B1).

The addition of these non-axisymmetric modes increases the number of degrees of freedom from the axisymmetric case by a factor of three such that it is now larger than the number of constraints (which are now all linear). This can be shown in general since for a toroidal field truncated at L_1, N_1 and a poloidal field truncated at L_2, N_2 the number of Taylor constraints is equal to half of the maximum degree of the polynomial in s [i.e. $C_T = \frac{1}{2}(L_1 + L_2 + 2N_1 + 2N_2) - 2$, Livermore *et al.* 2008] and the maximum number of Malkus constraints we have shown is given in terms of C_T by eq. (9). This results in a situation where if the poloidal field is fixed at a chosen resolution then for a toroidal field truncated quasi uniformly as $N = \mathcal{O}(L_{\max}) \approx \mathcal{O}(N_{\max})$ then we can see that the number of Malkus constraints scales as $\frac{9}{4}N^2$, which importantly, grows slower than the number of degrees of freedom for the non-axisymmetric linear system which scales as $3N^2$. Hence it is guaranteed that at a sufficiently large resolution toroidal field representation then there will be more degrees of freedom than constraints.

Therefore, barring degenerate cases, Malkus states exist. Compared with the case of a purely axisymmetric toroidal field, the number (but not the specific form) of linear constraints remains unaltered by the addition of these extra non-axisymmetric modes.

It is worth noting that the depth of the stratified layer does not enter into above derivation. The magnetic field solution in fact satisfies the Malkus constraints everywhere within its region of definition: in our case, this is the full sphere $0 \leq r \leq R$. □

Finally, we note that the above deviation is based upon a polynomial representation, which is sufficient for our purposes here. However, we know that any continuous function defined on a closed interval can be uniformly approximated as closely as desired by a polynomial function, and hence it can be extended to include an arbitrary magnetic field structure by expressing the relevant scalars in a polynomial basis of suitably large truncation.

APPENDIX C: ENUMERATION OF CONSTRAINTS

In order to determine the number of Malkus constraints, we calculate the maximum possible exponent in dimension of length within the Malkus integral. Since each constraint equation arises from ensuring a coefficient of a different exponent vanishes, enumerating all possibilities gives the maximum number of constraints.

There are three possible non-zero interactions whose sum comprises the Malkus integral, toroidal–toroidal, toroidal–poloidal and poloidal–poloidal as defined in eq. (B1). Since the poloidal field definition contains two curls whereas the toroidal field only one, then this extra derivative reduces the maximum exponent by one for interactions involving a poloidal field as opposed to a toroidal one. This means that the maximal case is determined by the toroidal–toroidal interaction, $[\boldsymbol{\mathcal{T}_1}, \boldsymbol{\mathcal{T}}_2]$. Since the Malkus integrand is identical to the Taylor integrand, we observe that the maximum radial exponent in the Malkus integrand $((\nabla \times \boldsymbol{\mathcal{T}_1}) \times \boldsymbol{\mathcal{T}_2})_\phi$ is $2L_{\max} + 4N_{\max} - 1$, as derived by Livermore *et al.* (2008). This is then reduced by two due to the property that the interaction of two toroidal harmonics that have identical spherical harmonic degrees and orders is zero (Livermore *et al.* 2008). This requires that one of the two modes has an $L_{\max}$ of at least one smaller than the other, hence resulting in a maximum possible degree in r of $2L_{\max} + 4N_{\max} - 3$.

Now under a transform in coordinate systems we note that r^n in spherical coordinates can be expressed as $s^j z^k$ in cylindrical coordinates, where $n = j + k$. Since only even values of j are present this results in $L_{\max} + 2N_{\max} - 2 = C_T$ non-trivial constraint equations in this dimension. There is no such restriction on k, which can take all values up to the maximum of $2L_{\max} + 4N_{\max} - 3 = 2C_T + 1$.

Each one of the constraints arises from a coefficient of a term with a different combination of exponents in s and z, explicitly, these terms have the following form:

$$\begin{aligned}&(A_{C_T,0}z^0 + A_{C_T,1}z)s^{2C_T} + (A_{C_T-1,0}z^0 + A_{C_T-1,1}z + A_{C_T-1,2}z^2 + A_{C_T-1,3}z^3)s^{2(C_T-1)}\\ &+(A_{C_T-2,0}z^0 + \cdots + A_{C_T-2,5}z^5)s^{2(C_T-2)} + \ldots\\ &+(A_{1,0} + \cdots + A_{1,2C_T-1}z^{2C_T-1})s^2 + (A_{0,0} + \cdots + A_{0,2C_T+1}z^{2C_T+1}).\end{aligned} \tag{C1}$$

Hence from the summation of the total number of these terms for every combination of j and k, with j even, such that $j + k \leq 2C_T + 1$ we have the following expression for the maximum number of Malkus constraints,

$$C_M = 2\sum_{n=0}^{C_T}(n+1) = (C_T+1)(C_T+2) = C_T^2 + 3C_T + 2.$$